Species, crown closure, and age as determinants of the vertical distribution of airborne LiDAR returns

Etienne Racine[1,*], Nicholas C. Coops[2], Jean Bégin[1], Mari Myllymäki[3]

[1]:Département des sciences du bois et de la forêt, 2405 rue de la Terrasse, Université Laval, Québec, QC G1V 0A6, Canada; [2]:Department of Forest Resources Management, 2424 Main Mall, University of British Columbia, Vancouver, BC V6T 1Z4, Canada; [3]:Natural Resources Institute Finland (Luke), Latokartanonkaari 9, FI-00790 Helsinki, Finland

Keywords: Boreal forest; LiDAR remote sensing; Tree Species; Functional data analysis; Stand structure.

Key Message

We assess even-aged stands vertical distributions of LiDAR returns and find that species, age, and crown closure each have a distinct pattern that explain up to 47% of the variations.

Abstract

Tree species have different shapes and forest stand dynamics. Light detection and ranging (LiDAR) can measure the three dimensional position of reflective material by sending laser pulses through the canopy. We examined the influence of three forest stand attributes: species, crown closure, and age on the vertical distribution of aerial LiDAR returns of forested stands. We studied over five thousand regular, even-aged stands in Quebec (Canada) with five dominant species: balsam fir (*Abies balsamea* (L.) Mill.), paper birch (*Betula papyrifera* Marsh), black spruce (*Picea mariana* (Mill.) BSP), white spruce (*Picea glauca* Moench) and aspen (*Populus tremuloides* Michx.). We modeled vertical distribution of LiDAR returns against the three attributes using a functional glm and a novel nonparametric graphical test of significance. Results indicate that aspen stands had the most uniform vertical distribution of LiDAR returns; balsam fir and white birch distributions were similar and centered around 50% of the stand height; black spruce and white spruce distributions were skewed below 30% of stand height (p<0.001). An increase in crown closure concentrated the distributions around 50% height. Increasing age gradually shifted the distributions higher in the stand until 50–70 years, where it plateaued and slowly declined at 90–120 years. The full model maximal R^2 was 0.47 around 10% of stand height. Results suggest that the stands vertical distributions of LiDAR returns depend on the three variables studied. This understanding can be used for stand-level species classification and to study the evolution of the forest structure over changing conditions.

1 Introduction

The distribution of vegetation material within canopies varies with tree allometry and competition strategies, leading to variations in canopy structure and ultimately in environmental conditions (Purves et al. 2007; Thorpe et al. 2010; Pretzsch and Dieler 2012). Species-specific canopy structures create different microhabitats, light conditions, and microclimates which in turn influence rates at which stands sequester carbon. Species

have different carbon allocation strategies that evolve during the growth season relative to above and below ground carbon allocation such as growing fruits, deploying leaves, or root access to nutrients and water (De Pury and Farquhar 1997; Lacointe 2000; Stark et al. 2012). These growth and allocation strategies result in the distinct species-specific tree shapes.

Traditionally, characterization of stand vertical distribution of aboveground biomass required either on-site estimation of biomass per vertical layer often using destructive measurements, scafolding, or tree climbing, that are time-consuming and limited to small areas (MacArthur and Horn 1969; Aber 1979; Bassow and Bazzaz 1997; Tackenberg 2007).

The increasing availability of data collected remotely from airborne, spaceborne and terrestrial sensors has improved our understanding of the forest dynamics (White et al. 2013; Wulder et al. 2012; Beland et al. 2019). Among these sensors, light detection and ranging (LiDAR) has the ability to penetrate the canopy and provide information on the spatial location of reflective material. LiDAR is increasingly used to perform both extensive and highly detailed imaging of the forest. It uses a laser whose location and orientation are precisely known to record a 3D scene. A discrete LiDAR pulse is reflected back to the sensor by the vegetation as it penetrates the canopy. The sensor then records the total travel time of the pulse and its energy to deduce the distance from the sensor to the location of reflection. LiDAR can be used from the ground, and from an aircraft to provide different perspectives on the forest. Terrestrial LiDAR provides highly detailed structural information of individual trees, but its extent is limited to hundreds of meters (Beland et al. 2019; Crespo-Peremarch et al. 2020). Airborne LiDAR, on the other hand, is generally used for extensive landscape measurements that are generally less detailed than terrestrial LiDAR.

Airborne LiDAR has been used to characterize vertical canopy structure, crown shape, and ecosystem's aboveground biomass (Lefsky et al. 2002; Parker et al. 2004; Coops et al. 2007; Stark et al. 2012; Harding et al. 2001; Cao et al. 2014; Ellsworth and Reich 1993; Papa et al. 2020), to identify tree species (Heinzel and Koch 2011, 2012; Vaughn et al. 2012; Axelsson et al. 2018; Hovi et al. 2016; Fassnacht et al. 2016; Budei et al. 2018; Fedrigo et al. 2018), and to study stand characteristics such as age, crown closure, and basal area (Korhonen et al. 2011; Racine et al. 2014; White et al. 2013). Airborne LiDAR is an important tool to quantify biomass and offers many opportunities to explore large-scale phenomena that could only be observed on the field, such as large-scale habitat characterization (Vierling et al. 2008, 2010; Seavy et al. 2009).

One of the limitations of the small footprint LiDAR sensor is its inability to distinguish differences in foliage condition or species spectral variations because it lacks spectral information commonly used to classify species such as variations in color or near-infrared. In response, the most common strategy to distinguish species with LiDAR has been to rely on individual tree shapes and texture (Holmgren and Persson 2004; Kim et al. 2011; Fassnacht et al. 2016), add spectral information by supplementing it with spectral imagery, and more recently using a multispectral LiDAR (Budei et al. 2018; Budei and St-Onge 2018).

Most studies on species classification using aerial LiDAR have focused on individual tree-crown species identification. Tree crown delineation requires a high number of LiDAR returns and very accurate registration of ground observations (Ørka et al. 2009; Muss et al. 2011). Furthermore, a small observation area such as an individual tree crown loses the shape of the vertical distribution of LiDAR returns because the number of LiDAR returns decreases and the distribution increasingly becomes a collection of random deviates. For that reason, species identification accuracy is improved by having a very high point density in excess of 10 pt/m^2 (Fassnacht et al. 2016) making it difficult to apply and validate these approaches over large areas, and on a less dense LiDAR datasets.

An alternative to individual tree-crown extraction approaches is the application of area-based approaches (see e.g. White et al. (2013)). This approach generally uses a pixel or a stand on which LiDAR returns are aggregated and from which predictors are derived and then used in a model to predict forest attributes. LiDAR metrics often derive predictors from the vertical distribution of LiDAR returns: the number or LiDAR returns per height slice. The vertical distribution of LiDAR returns is often presented as quantiles, projections of quantiles (such as principal component analysis), or parametric functions (such as a Fourier, beta or Weibull functions), which are used to predict stand attributes (Mehtätalo 2006; Coops et al. 2007; Racine et al. 2014; Maltamo et al. 2005; Palace et al. 2015; Magnussen et al. 1999; Riggins et al. 2009; Falkowski et al. 2009). The area-based method can be effective with point density as low as 1 pt/m^2, which reduces cost and

processing compared to tree-crown approaches (White et al. 2013).

Lowering the minimum LiDAR point density threshold for species classification would increase the number of potential surveys where the method could be applied while reducing the costs of acquisition. The species information could then be used for extensive forest management, or landscape-scale studies. One avenue to area-based species mapping is to increase our understanding of the interaction between LiDAR and stand-level vegetation. The vertical distribution of LiDAR returns is complex to analyze without resorting to dimension reduction, a method that generally limits the interpretability of results. We hypothesize that using functional general linear models (GLM) and a novel non-parametric graphical test of significance (Mrkvička et al. 2019) would allow to link the forest attributes to the vertical distribution from low-density LiDAR surveys. The test provides a framework to compare a function (i.e. the vertical distribution of LiDAR returns) against categorical and continuous variables. It allows for a visual understanding of the effects of the variables on the functional data.

The information contained in the vertical distribution of LiDAR returns is closely related to the distribution of the vegetation. Reduced crown closure (the proportion of area covered by vegetation) generally allows for an increased probability for the LiDAR returns to reach lower vegetation (Hilker et al. 2010). In turn, age influences the vertical position of the crown within the stand (Coops et al. 2009; Racine et al. 2014). While using direct foliage measurements, Aber (1979) observed that the vertical concentration of the foliage evolved across stand age, and that the end point of the forest succession seemed to reach an equilibrium where the foliage was relatively evenly distributed within the canopy. Martin-Ducup et al. (2016) noted that crown closure and stand maturity affected the shapes of the crown of sugar maples as measured using terrestrial LiDAR.

Species shapes influence the distribution of LiDAR returns, but most studies interpretations are limited and hard to generalize across ecosystems or LiDAR surveys (Fassnacht et al. 2016). Some studies explicitly compared the vertical distribution of LiDAR returns between species. For example, Ørka et al. (2009) found that the first and last returns were more dispersed in Birch (*Betula* spp.) stands than in Norway spruce (*Picea abies* (L.) Karst.), which also had a vertical distribution of first returns skewed toward the superior canopy, and that increased stand height modified the overall return distribution. To our knowledge, it is the first time that a functional GLM combined to a non-parametric graphical test of significance is used in ecology or remote sensing, although similar graphical tests have been applied to economical data (Mrkvička et al. 2020), and similar non-parametric inference is commonly used in neuroimaging (Winkler et al., 2014).

In this study we verify if we can discriminate distinct patterns between species in the vertical distribution of LiDAR returns from a low-density area-based survey. We hypothesize that the use of a functional GLM combined to a non-parametric graphical test of significance makes it possible to verify inter-specific differences in the vertical distribution patterns after accounting for stand crown closure and age effects.

2 Method

2.1 Study area

The study was conducted in Matane Wildlife Reserve (Quebec, Canada, 48°41'N, 66°58'W) covering 1600 km^2 (Figure 1). The Reserve is a mixed forest mostly dominated by balsam fir (*Abies balsamea* (L.) Mill.), paper birch (*Betula papyrifera* Marsh), and black spruce (*Picea mariana* (Mill.) BSP), but other species are present such as white spruce (*Picea glauca* Moench), aspen (*Populus tremuloides* Michx.), Norway spruce (*Picea abies* (L.) Karst.), jack pine (*Pinus banksiana* Lamb.), and other non-commercial deciduous species. Most of the Reserve is under active commercial logging, which was documented since 1962: 27% of the area had been harvested (mostly total harvesting) of which half of the areas had been replanted. Other natural origins (e.g. windthrow, insect epidemic, fire) accounted for 2% of the territory and the remaining 71% of the territory had an undocumented origin.

Figure 1: Location of Matane Wildlife Reserve (left panel) and selected stands within the study area (right panel, dark patches).

2.2 Data

Airborne imagery and LiDAR were acquired during the summer of 2007. All data were collected by the Quebec Ministry of Natural Resources as part of their decennial forest mapping program. LiDAR survey had a nominal point density of 3 points/m^2 with an Optech ALTM 2050 sensor recording first and last returns at 40kHz, flown at 1200 m above ground, with a flight overlap of 30% and maximal scan angle of 15° from nadir with a footprint diameter of 25 cm.

Airborne photography was acquired with a Leica ADS–40 pushbroom camera at a resolution of 0.2 m for panchromatic, and 0.5 m near-infrared, green, and blue bands (NIR, G, B respectively centered on 860, 560, and 460 nm); side overlap was 40% to ensure complete coverage of the area. This imagery was interpreted into stands following provincial guidelines adapted from MRNQ (2007) by expert photo-interpreters. Using digital stereopsis (virtual 3D vision) from the forward and nadir-facing ADS–40 sensor images, the expert photo-interpreter classified many species by integrating information on landscape position, crown shapes, texture, and color. Every photo was segmented into homogenous stands using species, crown closure, height, and geomorphic criteria. Each stand was classified regarding species composition, crown closure, age, height, and other ecological variables using a combination of photography, ground-control points and historical data as a reference. Stand age is estimated using ground control plots where trees were cored, this information is then combined with available archives, height, and ecology to judge age from aerial photography. Forest age is interpreted in 7 regular: (10 [0–20], 30 [21–40], 50 [41–60], 70 [61–80], 90 [81–100], 120 [101, ∞]), and irregular age classes. Crown closure is visually estimated by comparing the proportion of open ground with the space occupied by the mature tree crowns. It is estimated in 9 classes: 10 [5–14], 20 [15–24], 30 [25–34], 40 [35–44], 50 [45–54], 60 [55–64], 70 [65–74], 80 [75–84], and 90 [85–100]. Species are identified by their distinctive spectral response based on composite near-infrared image, green and blue (NIR+G+B) images respectively mapped to red, green, and blue (R, G, B) channels, and their frequent associations in forest stands (Table 2.2). Finally, the interpretation relied on the ground-control points and the ecological knowledge of the photo-interpreter. We used this photo-interpreted forest map as our reference data for species, crown closure, and age.

Description of tree shapes and associated species

Species

Silhouette

Interpretation description[1, 2]

Associated species[1]

Abies balsamea

Mesic sites. Narrow conic crown with a sharp and thin summit that is frequently pale because of the accumulated cones that are more reflective than foliage. Brown, slightly pink tint, browner and pinker than white spruce.

Trembling aspen, white birch, white spruce, black spruce, red spruce, and eastern hemlock.

Betula papyrifera

Multiple conditions but avoids poorly drained sites. Shaped as a flat half-sphere. Crowns are also highly mingled and present an irregular texture that makes them hard to identify individually even at higher resolutions. Dark pink tint between yellow birch and maples.

Various species such as other birches, pines, spruces, hemlocks, poplars, maples, balsam fir, northern red oak, and pin cherry.

Picea mariana

On poorly drained sites, crown thin and narrow, spirelike, sharp summit with compact foliage. On well-drained upland sites, principal branches short compared with other spruces, lower ones greatly drooping, tips upturned. Upper part of the crown often very dense, oddly shaped, with many cones. Brown, slightly pink when young, paler than white spruce.

In the southern part of its range, tamarack. Northern part: jack pine, white spruce, balsam fir, white birch, trembling aspen.

Picea glauca

Well to moderately drained sites in mid slopes. Broad conical crown, appears star shaped, ragged, irregular, densely foliated, spirelike in northern parts of its range. Principal branches bushy, generally horizontal, sometimes sloping downward in the lower part of the crown, tips gradually upturned. Brown, slightly pink when young, darker than black spruces.

Trembling aspen, white birch, black spruce, and balsam fir.

Populus tremuloides

All sites except poorly drained. Short, rounded, light bulb-shaped crown usually taller than surroundings when mixed. Crown surface looks blurred and smooth because of the small leaves. Orange-tinted pink.

White spruce, black spruce, balsam fir, white birch, balsam poplar and jack pine

1 Colors are based on (NIR+G+B mapped to R, G, B channels).

2 Adapted from Farrar (1995) and Leboeuf and Vaillancourt (2013)

2.3 LiDAR Data Processing

Even-aged stands are less complex to analyze from a vertical structure point of view than irregular stands, so we focused our analysis on even-aged stands with clearly dominant species representing at least 50% of the stand cover. The steps required to prepare LiDAR data for processing are sumarised in Figure 2. We excluded stands with an average LiDAR sampling rates below 2 pt/m^2 or an area of less than 4 ha to ensure sufficient number of LiDAR returns. From these stands, we kept only those with a dominant species that had at least 100 observations (stands): aspen, balsam fir, black spruce, paper birch and white spruce. From 22 365 stands of the original forest map, we reduced our dataset to 5 428 stands representing 35% of the study area (Figure 1). Stand area distributions were similar for all selected species (median 9 ha, minimum 4 ha, maximum 137 ha).

We registered the LiDAR returns in a common vertical system to make them comparable. We subtracted the ground elevation from the absolute point elevation to compute the vertical distribution of LiDAR return for every stand (Muss et al. 2011). Vertical distribution is a histogram of LiDAR returns height sliced in 40 horizontal sections relative to their highest returned point. The slices were defined relative to maximal height (Coops et al. 2007; Harding et al. 2001) to allow comparison across stands of different heights. We then divided each slice count by the total number of points of the stand so each stand vertical distribution summed to one to allow comparisons between stands of inconsistent shapes, areas, and LiDAR point density.

2.4 Satistical Analysis

We used a novel method that builds on the functional data analysis field (Ramsay and Silverman 2005) to compare the complete vertical distribution of LiDAR returns. Most studies of species classification have focused on the accuracy of classifiers and the value of predictors for classification (Fassnacht et al. 2016), often using dimension reduction to decrease and decorrelate the number of predictors such as linear discriminant analysis or principal component analysis (Koenig and Höfle 2016; Räty et al. 2016; Axelsson et al. 2018). However, dimension reduction decreases the ability to understand the effect of a given variable and interpret the results of the model.

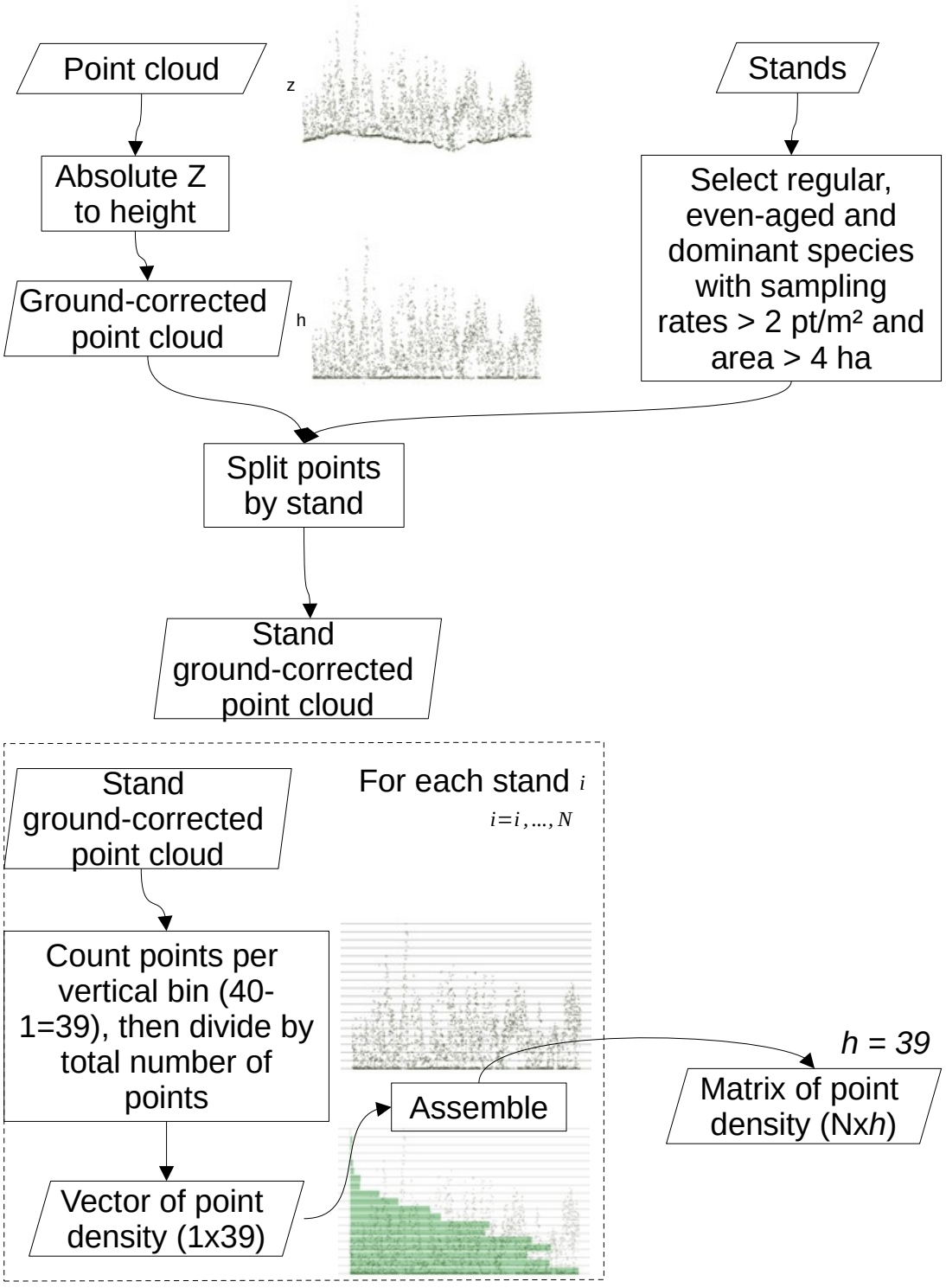

Figure 2: Preparation of the LiDAR data

To compare inter- and intraspecific variations in the distribution of LiDAR returns and the confounding variables, we used a nonparametric graphical test of significance (Myllymäki and Mrkvička 2019; Mrkvička et al. 2019) (Figure 3). We modeled the vertical distributions of LiDAR returns as a function of dominant species, crown closure, and age using the general linear model

$$d_i(h) = \beta_0(h) + \beta_{sp}(h) \cdot Species_i + \beta_{cc}(h) \cdot CC_i + \beta_{age}(h) \cdot Age_i + \varepsilon_i(h) \quad (1)$$

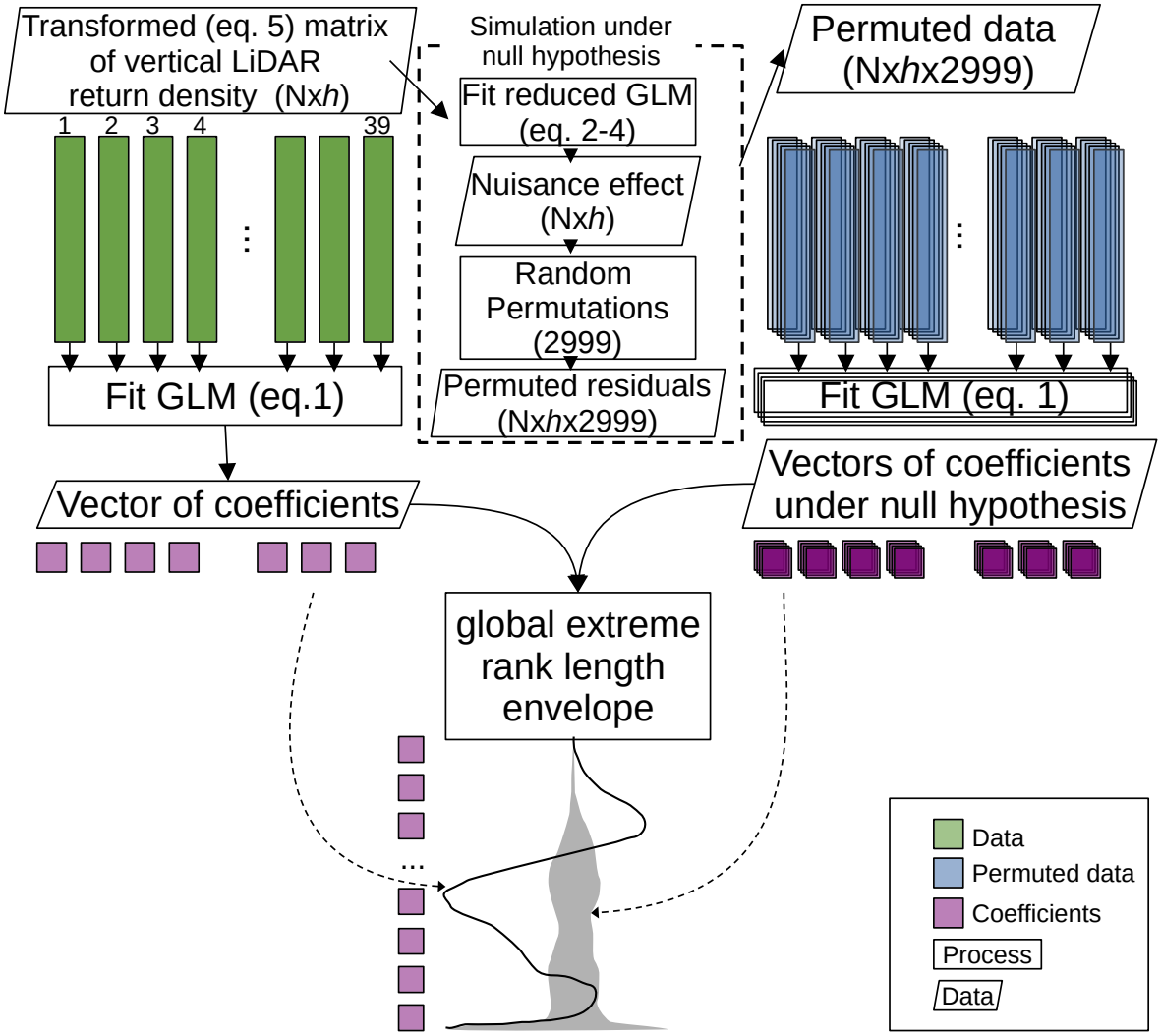

Figure 3: Analysis of the vertical distribution of LiDAR returns

where d_i contains the LiDAR density distribution at scaled height h (represented by the vertical distribution histogram) for observation i, and $\beta(h)$ is the parameter vector related to each variable, CC is crown closure, and $\varepsilon(h)$ is the error term with mean zero and finite variance σ^2. Species as well as age—given that the last class was open—were regarded as categorical variables and thus encoded with dummy variables in $Species_i$ and Age_i, while CC_i was regarded as a continuous variable.

We studied the effect of each variable after accounting for the other confounding variables (also called the nuisance factors by Freedman and Lane (1983)). We tested the three null hypotheses $\beta_{sp,m}(h) = 0$ for all m and h, $\beta_{cc}(h) = 0$ for all h, and $\beta_{age,l}(h) = 0$ for all l and h for the three variables, respectively. For the discrete factors, m and l are equal to the number of groups of the discrete factor and the coefficients were

constrained to sum to zero. The corresponding three null models were obtained by removing the studied variable from the full model (Equation (1)),

$$d_i(h) = \beta_0(h) + \beta_{cc}(h) \cdot CC_i + \beta_{age}(h) \cdot Age_i + \varepsilon_i(h) \tag{2}$$

$$d_i(h) = \beta_0(h) + \beta_{sp}(h) \cdot Species_i + \beta_{age}(h) \cdot Age_i + \varepsilon_i(h) \tag{3}$$

$$d_i(h) = \beta_0(h) + \beta_{sp}(h) \cdot Species_i + \beta_{cc}(h) \cdot CC_i + \varepsilon_i(h) \tag{4}$$

We used the coefficients of the variable of interest (the left-out β in Equations (2)–(4)) for the statistical test as suggested by Mrkvička et al. (2019): for the continuous crown closure variable, the test statistic was the vector $\beta_{cc}(h)$ for all h; for age, the test was based on the values of the effect $\beta_{age,l}(h)$ of all the age groups l for all h. To inspect species differences, another alternative was used: the test was based on all differences $\beta_{sp,m}(h) - \beta_{sp,n}(h)$ for species m and n with $1 \leq m < n \leq 5$.

The test relies on two procedures: 1) Freedman-Lane algorithm to permute the residuals of the null model and create the reference distribution of the coefficients under the null hypothesis, and 2) the *global extreme rank length envelope test* to build a null global envelope for the above mentioned test statistics and correct for the multiple tests conducted along h (Myllymäki et al. 2017). The Freedman-Lane algorithm includes all steps from the Simulation under the null hypothesis to the estimation of the coefficients under the null hypothesis (Figure 3).

The null hypothesis was rejected if the test vector, calculated from the vertical distribution of LiDAR returns, leaved the envelope at any point. We used 2999 random permutations to estimate the p-value and to build the global envelopes for the nonparametric graphical test of significance (Myllymäki and Mrkvička 2019). To account for the tests of all three variables, we used a Bonferroni adjusted significance level $\alpha = 0.05/3$ in addition to the inherent correction applied within the *global extreme rank length envelope test* to account for multiple h, and consequently considered the 98% global envelopes. We checked the data for heterogeneity of variance (Winkler et al. 2014), and the model residuals indicated heterogeneity of variance for all variables. Following Mrkvička et al. (2020), we transformed the matrix of vertical LiDAR return density (Figure 3) by scaling groups (j) according to their variance dispersion. The initial $d_{i,j}$ function was transformed into $S_{i,j}$ function,

$$S_{i,j}(h) = \frac{d_{i,j}(h) - \bar{d_j}(r)}{\sqrt{Var(d_j(h))}} \cdot \sqrt{Var(d(h))} + \bar{d_j}(h) \tag{5}$$

where the group sample variance $Var(d_j(h))$ is used to correct for unequal variance among groups. The group sample mean $\bar{d_j}(h)$ and overall variance $Var(d(h))$ are used preserve the original scale of the mean and variability of the functions.

Our experiments with simulated data showed that the application of the transformation for all groups at once (by combining all group levels) generally removed heterogeneity of the variance, but it required to have sufficient observations in all categories, which was not the case of our data. We instead relied on the successive application of the transformation (Equation (5)) for each of the confounding variables. In this case, we found that the order in which the transformation is applied is important because it can reintroduce heterogeneity of variance. We settled on the successive transformation by crown closure, age, and species which provided the best results and reduced heterogeneity. We verified the importance of the correlation by running Breusch-Pagan (Breusch and Pagan 1979) test of heteroscedasticity using the squared residuals $(d_i(h) - \hat{d}_i(h))^2$ on the left-hand side of the reduced equations (2)–(4). While the test indicated significant heteroscedasticity in some areas of the curves, the coefficient of determination was less than 4% for all variables and all h, which confirmed that no further adjustment was required.

We performed the analysis using R 3.6.3 (R Core Team 2020), the GET package (Myllymäki and Mrkvička 2019; Mrkvička et al. 2019), and Lastools (Isenburg 2012) to correct and extract the LiDAR data.

3 Results

The contrasts from the nonparametric graphical test of significance confirm that we can reject the null hypothesis: the differences between all species, after accounting for age and crown closure, were significantly different ($p < 0.001$) (Figure 4). We observed two groups of species where differences were significant but small: balsam fir–paper birch, and black spruce–white spruce. Balsam fir and paper birch differences were small and localized at 65–70% and below 12% of stand height. White spruce and black spruce also had small localized differences at 22–30% and 5–8% of stand height. However, some differences were more important between groups of species (indicated by the bold lines in Figure 4): black and white spruces had the lowest distribution of LiDAR returns when compared to other species. Black spruce had fewer returns than balsam fir between 38–62% of stand height (40–57% for paper birch), while it had more below 28% of stand height (30% for paper birch). Aspen's vertical distribution of LiDAR returns had a significantly distinctive shape when compared to every other species: it did not display a prominent peak, which made the distribution more uniform than other species (Figures 5 and 6). Except for the area between 57–60% of height for all species, and 8–18% for balsam fir and paper birch, all differences with aspen were significant (p<0.001). Overall, areas of larger differences for species were located around 5, 25, 50, and 70% of stand height.

An increase in crown closure was associated with a decrease in the density of LiDAR returns below 33% of stand height, while the density of LiDAR returns above 38% increased (Figure 7). The largest augmentation was concentrated around the middle height (50%), while the inferior area (around 3% of height) had the largest reduction effect. Figure 5 displays the effect of crown closure on each species vertical distribution of LiDAR returns, including the effect of age. The increase in crown closure concentrated the returns around the middle height, except for aspen which peak was located superior (around 80% of stand height) and white spruce which peak was inferior (around 20%). Although black spruce peak was centered at 50% stand height for high values of crown closure, the observed variability was skewed toward the inferior stand height. Some species were more represented in younger or older age classes, which inflated the variation envelopes. The model from Figure 7 accounted for this effect.

The effect of increasing age gradually shifted the distribution higher in the stand up to 70 years of age, when it seemed to reach a plateau (Figure 8). The effect of age was significant at most height for stands between 10 and 70 years of age, while significant effect for stands of 90 and 120 years of age were of smaller magnitude and below 69% and 44% respectively (p<0.001). The gradual shift of the distribution toward the top of the stand as age increased is reflected by the younger stands (10, 30 yr) with an abundance of lower returns below 28% and 41% respectively, and fewer returns above 33% and 49% of height, respectively. The effect is reversed in mature stands of 50 and 70 years, where age inflated the distribution between 38–97% of stand height (44–100% for 70 yr), and deflated it below 31% of stand height (38% for 70 yr). Like mature stands, older stands of 90 and 120 years of age also had an abundance of returns in the superior part of the stand, although it was lower than mature stands (90 yr: 38–68%; 120 yr: 33–44%) and of smaller magnitude. Older stands vertical distribution were reduced below 28 and 23% of stand height for 90 and 120 years of age, respectively. Overall, the rate of change in the vertical distribution of LiDAR returns gradually decreased as the age increased. For example, changes in the distribution between 10 and 30 years were larger than the changes between 70 and 90 years. Overall, areas of higher variability for age groups were located around 5, 20, and 50% of stand height. Figure 6 displays the effect of age on each species vertical distribution of LiDAR returns. The young white and black spruces stand displayed a strong asymmetry toward the inferior part of the stand that disappeared in older stands.

The coefficient of determination of the models varied across stand height (Figure 9). The most correlated areas for every model were around 5–15%, and 46–54% of stand height, while all models displayed a sharp decline between 28–40%. The highest R^2 was for the full model at 0.47 (at 10–13% of height) and 0.42 (at 49–51%). The model explicitly excluding the species variable (Eq. (2)) displayed a difference of more than 0.10 with the full model R^2 between 72–92% stand height. Excluding the crown closure variable from the model (Eq. (3)) created a difference of more than 0.10 with the full model R^2 between 0–21% and 46–67% of stand height. The model excluding the age variable (Eq. (4)) displayed a difference of more than 0.10 with the full model R^2 at 18–38% and 62–64% of stand height.

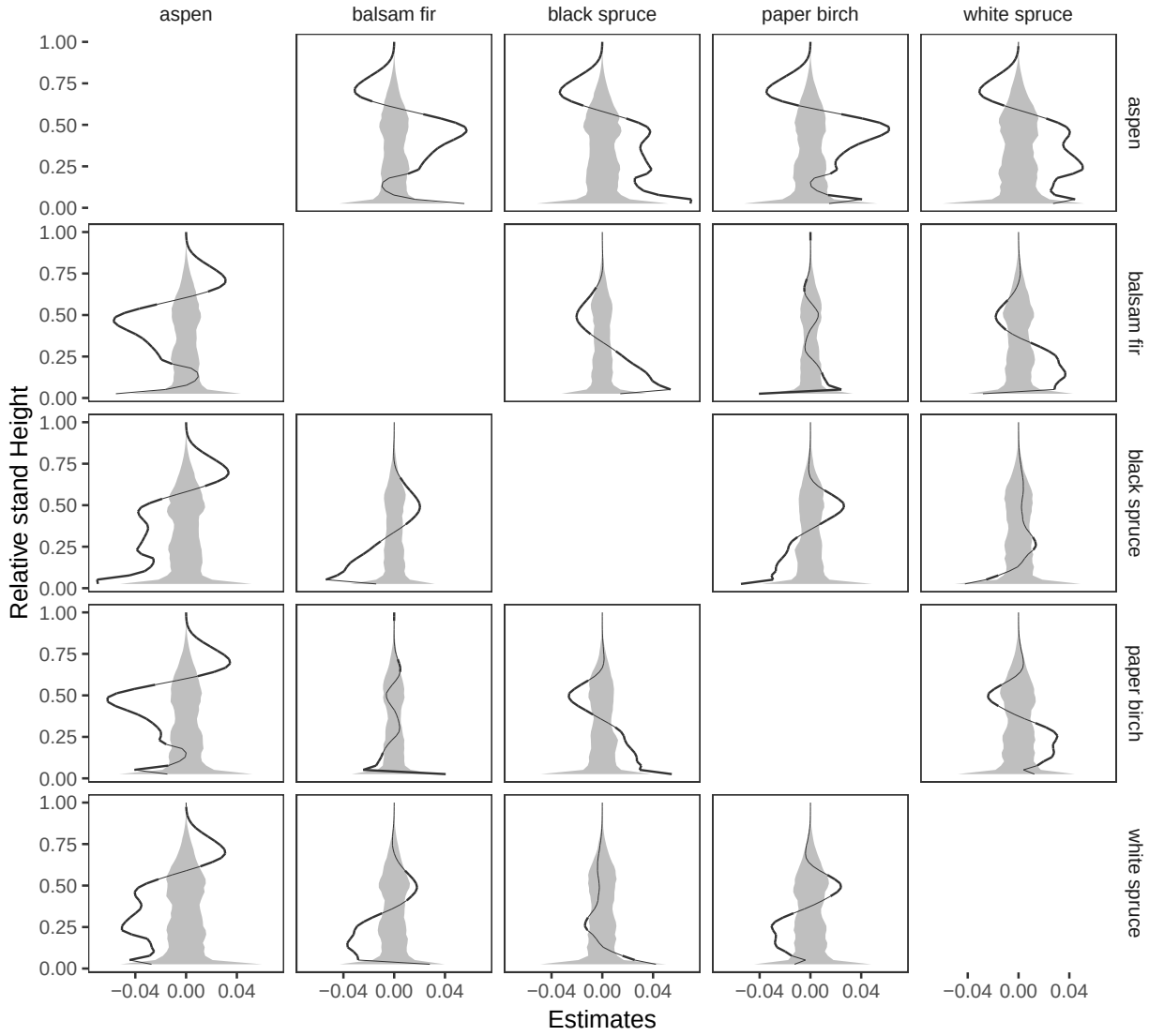

Figure 4: Nonparametric graphical tests of significance for species using contrasts: the observed difference between the coefficients of two species (black curve), where species in rows are subtracted from the species in columns (e.g. first column, second row is the aspen − balsam fir contrast), and the 98% global envelope (grey bands below the diagonal) that shows the area of acceptance of the null hypothesis (no effect, $p<0.001$) obtained from the permutations of the residuals of the null model (Equation (2)). The observed curve is bolder when outside the envelope. Panels above the diagonal are the reflection of the observed functions and the global envelope from the lower part.

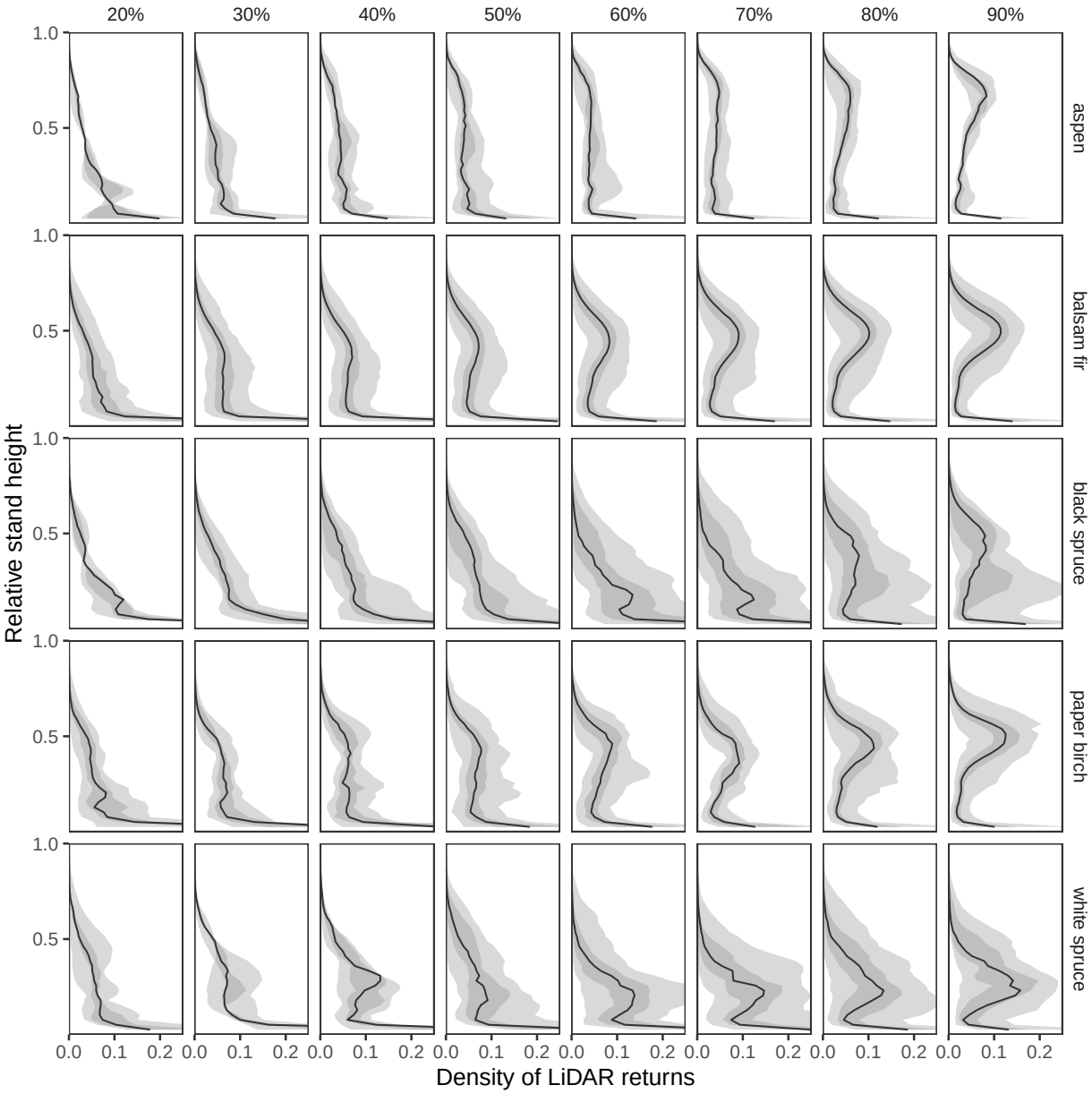

Figure 5: Vertical distribution of LiDAR returns as a function of crown closure (columns) and species (rows). Black lines represent the median distribution; shaded areas represent 95% and 50% local variation envelopes.

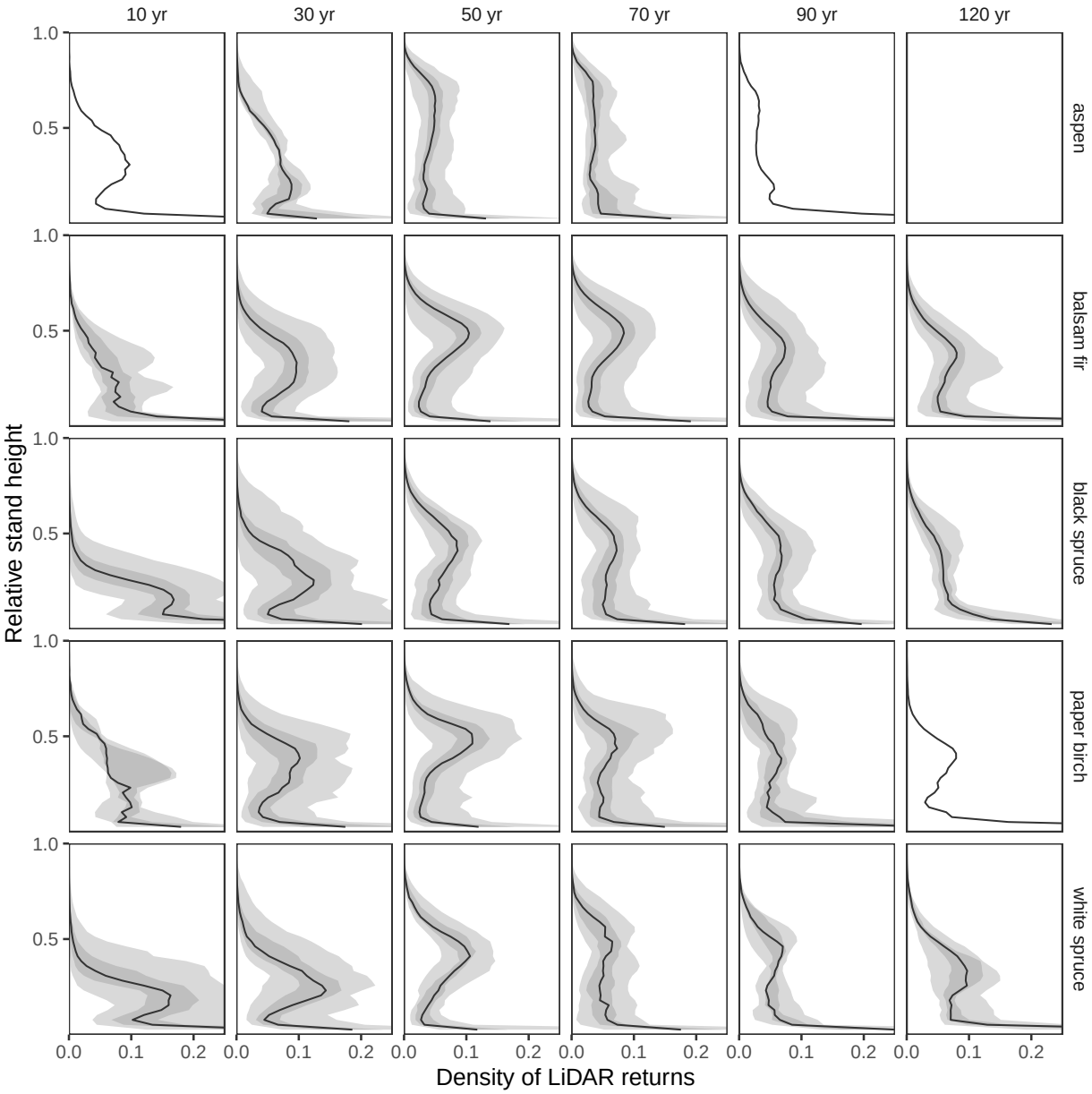

Figure 6: Vertical distribution of LiDAR returns as a function of age (columns) and species (rows). Black lines represent the median distribution; shaded areas represent 95% and 50% local variation envelopes.

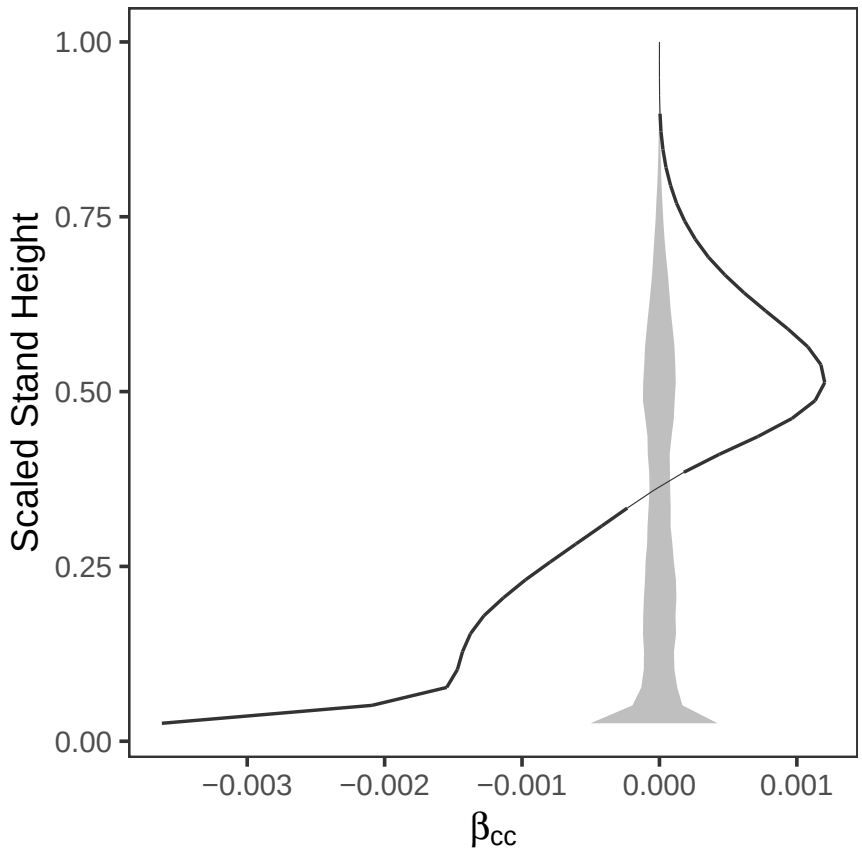

Figure 7: Nonparametric graphical tests of significance for crown closure: the observed coefficient (black curve), and the 98% global envelope (grey band) that shows the area of acceptance of the null hypothesis (no effect, $p<0.001$) obtained from the permutations of the residuals of the null model (Equation (3)). The observed curve is bolder when outside the envelope.

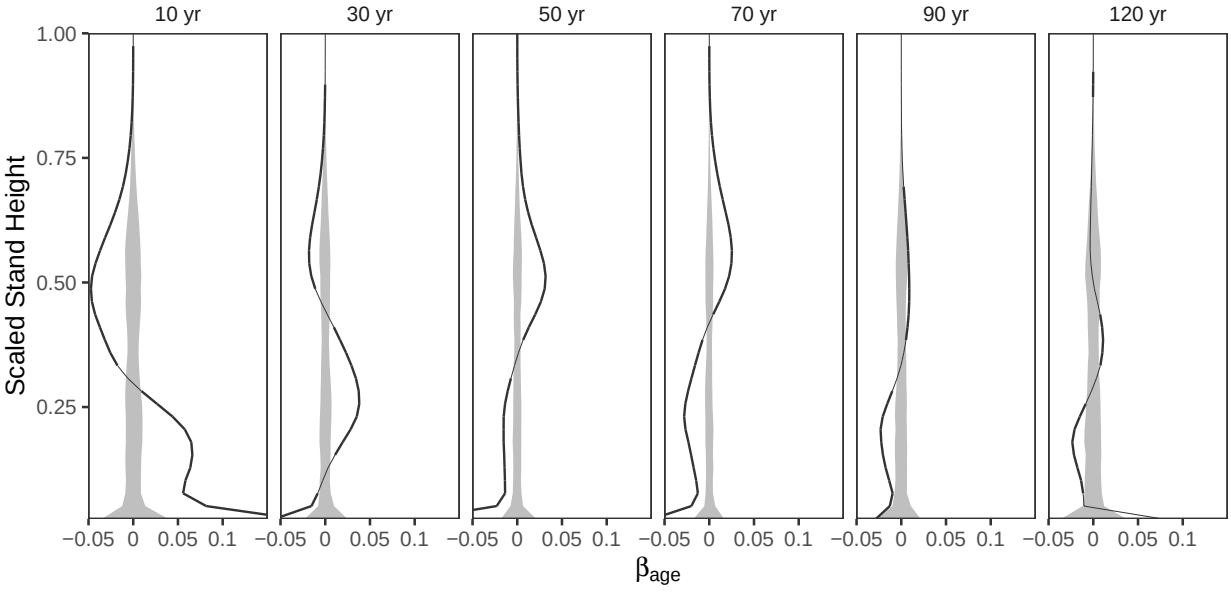

Figure 8: The nonparametric graphical tests of significance for age: the observed coefficients of the six age groups (black curves), and the 98% global envelope (grey bands below the diagonal) that shows the area of acceptance of the null hypothesis (no effect, $p<0.001$) obtained from the permutations of the residuals of the null model (Eq. (4)). The observed curve is bolder when outside the envelope.

4 Discussion

Our objective was to study the influence of species, crown closure and age on the vertical distribution of LiDAR returns. We found that even-aged stands exhibit species-specific patterns that evolve predictably with crown closure and age. We observed two groups of species: balsam fir and paper birch which had a more symmetrical vertical distribution of LiDAR returns centered between 40 and 60% of stand height, and white spruce and black spruce distributions of LiDAR returns that were generally skewed toward the inferior part of the stand (below 30%). Aspen displayed a more even distribution of LiDAR returns with a higher proportion of returns in the superior part of the stand than other species.

While individual trees are all plastic and opportunistic, adapting to specific light and environmental conditions, we found that stands of a species exhibit similar vertical characteristics that distinguish them from other species. This observation is consistent with previous field observations conducted on a smaller area with different measurement methods (Purves et al. 2007). However, we expected clearer patterns along a shade-tolerance gradient or conifer versus deciduous; we found that patterns of paper birch were more similar to balsam fir than aspen, another shade-intolerant deciduous, while balsam fir is a shade-tolerant conifer. Since we used the dominant species to classify stands, this could be the result of frequent association between balsam fir and paper birch in the same stand.

Increased crown closure was associated with a concentration of the vertical distribution of LiDAR returns which moved points below 33% to above 38% of stand height. Complementarily, stands with a lower crown closure presented a vertical distribution of LiDAR returns that was more dispersed and skewed toward the ground, with fewer returns in the superior part of the stand. This effect was also apparent when comparing the variance explained by the models in Figure 9 where crown closure appeared to contribute to explain at least 25% from the variance explained by the full model below 21% and between 44–69% of stand height.

Age increase was associated with a displacement of the vertical distribution of LiDAR returns to the top of the stand for up to 50–70 years and then plateaued or declined in the 90–120 years groups. The rate of change between age groups decreased as the age increased: younger stands vertical distribution of LiDAR returns

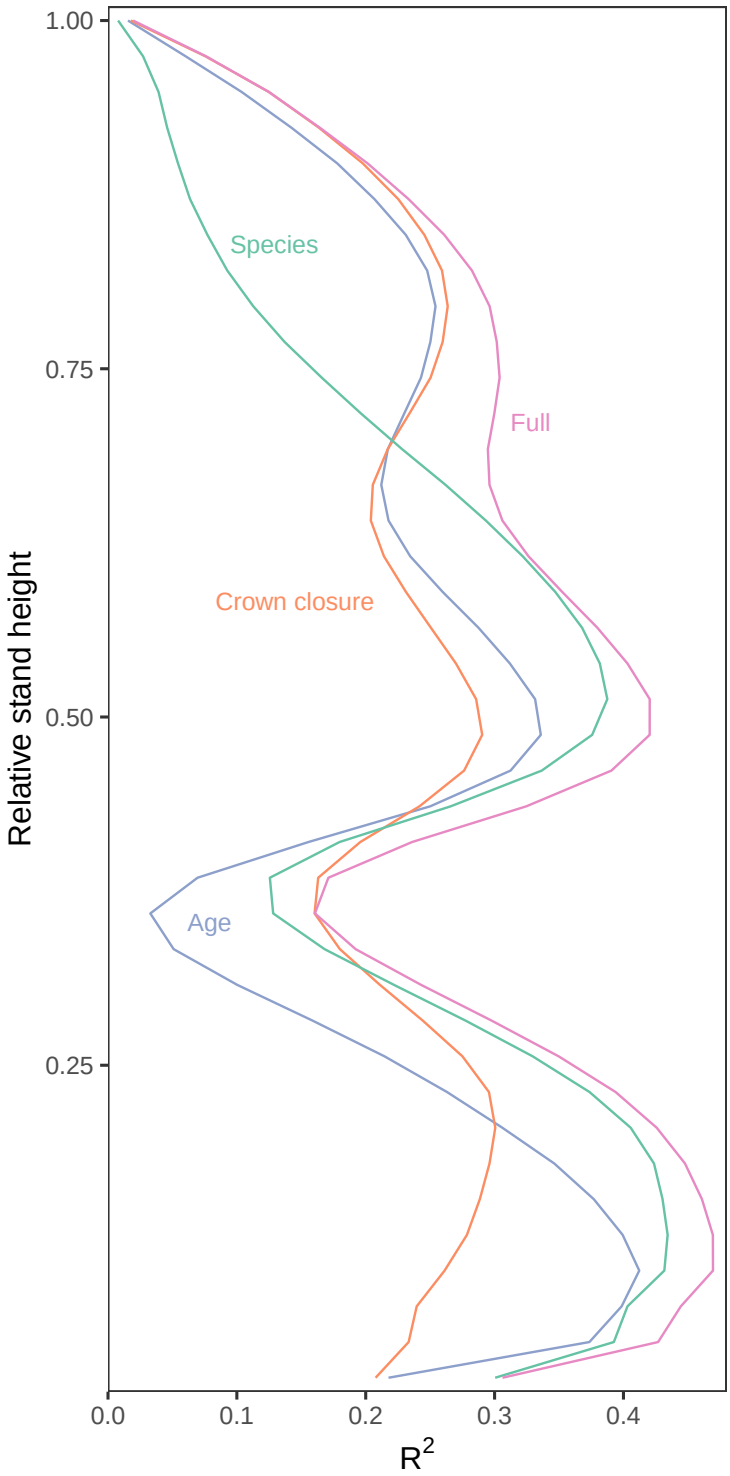

Figure 9: Comparison of $R^2(h)$ of the full model (Eq. (1)) containing all variables, and the three reduced models (Eq. (2)–(4)) where one variable has been left out (either Species, Crown Closure, or Age).

appeared to undergo a rapid transformation in the 10 yr group, which gradually decelerated to stabilize in the 70 years group. The 90 and 120 years groups displayed the smallest magnitude of change. While it is well established that absolute stand height varies predictably with age, the changes we observed here are relative to the maximal height of the stand. Age effect was akin to the crown closure effect: while they increased, they were both associated to an increased proportion of points in the superior part of the stand. The crown closure variable however seemed to explain more of the distribution variations in the lower stand (below 21%) and the middle stand (46–67%), while age contribution to R^2 happened between 18–38%. Unlike Aber (1979) who observed a stable distribution of foliage at the end point of the forest succession, the vertical distribution of LiDAR returns of the 120 year class rather displayed a marginal concentration below the middle height (33–38%).

The most important differences between vertical LiDAR distributions occurred below 80% of height. The superior sections of the stand often displayed very small differences in distributions while the inferior portion displayed large variations. The distribution of LiDAR returns in the superior and inferior portions of the stand can be highly dependent on the LiDAR survey parameters (Roussel et al. 2017, 2018), which might make them less likely to be stable across different surveys. Nonetheless, the full model (Eq. (1)) still explained 20% of the variability up to 90% of stand height. The difference in variability explained by the species model compared to the full model was more important above 72% and peaked at around 80% (Figure 9). One possible explanation is that the area 74–90% is associated to important differences between aspen and all other species, which were probably not explained by crown closure or age.

The area 31–46% of stand height exhibited a sharp decline in R^2, where age seemed to explain most of the variance of the full model. While the reasons for this sharp drop are unknown, the area is associated with an increase in LiDAR returns for stands of the 120 yr group and seems to be a transition area for the spruce group and the balsam fir–paper birch group between an inferior–skewed distribution and a centered distribution. The meeting of these two distributions might create noise which might be amplified by the registration of the curves—scaling the curves relative to the highest return received.

Interestingly, the graphical test of significance rejected the hypothesis that the distributions of LiDAR returns were similar, and also identified the areas responsible for the rejection. This allowed to form groups of species with similar distributions. We think that this method could complement and sometimes replace other methods of analysis of the vertical distribution of LiDAR returns, such as principal component analysis or linear discriminant analysis when interpretability is desired.

4.1 Limitations

The median stand area was 9 ha, a large area compared to other area-based approaches, which allowed the aggregation LiDAR returns to identify specific patterns. Stands are by design the most homogeneous unit of the forest landscape and vertical LiDAR distributions are more reliable after a sufficient number of aggregated returns are grouped. The exact optimal area to observe these patterns will require additional research.

The vertical distribution of LiDAR returns for each stand was scaled using the highest LiDAR return. This could make the registration sensitive to extreme measures and might explain, in part, why the superior part of the canopy's R^2 was lower. In young stands, where a single mature tree might remain, the distortion of the vertical distribution of LiDAR returns could be high and reduced as the trees approach their maximal height for the site. Using a high quantile rather than the highest return could reduce this effect. Nonetheless, the variance explained by the model using highest–point registration still proved useful.

The non-parametric graphical test of significance that we used is slightly liberal because the Freedman-Lane permutation is approximate (Mrkvička et al. 2019), however, the permutation scheme is regarded as one of the best methods from the literature under the presence of confounding variables (Anderson and Robinson 2001; Winkler et al. 2014). It also has the advantage of the graphical interpretation, especially the identification of the area of rejection, which allowed us to interpret at which relative heights and between which species the differences occurred.

4.2 Future outlook

We found differences in the distributions of LiDAR returns of five tree species. The graphical test of significance allowed an interpretation of the vertical distribution of LiDAR returns, which could be used to improve our understanding of stand structure evolution and species classification with LiDAR. In a review of remote sensing tree species classification, Fassnacht et al. (2016) noted that most studies pursued the optimization of classification accuracy, and provided little analysis of the causal understanding of species discrimination. Although we did not perform species classification, our results show that it is possible to interpret the differences between complex predictors such as the vertical distribution of LiDAR returns while accounting for confounding factors.

Additional evidence is needed to establish if the relation between vertical density of LiDAR returns, and species, crown closure, and age are circumstantial to our study area, or if they hold in other areas, with different species, and LiDAR survey parameters. Other variables, such as LiDAR scan angle and abiotic factors, could be included to improve the model.

Our results indicate that LiDAR vertical distribution can be analyzed using a graphical test of significance. These results can be used extensively to study forest structure on a new scale.

5 Conclusion

Using light detection and ranging (LiDAR) vertical distributions can provide an understanding of the interplay between species, crown closure, and age. The use of the functional generalised linear models combined to the graphical test of significance allows interpreting the differences in distributions explained by multiple confounding variables. By using an airborne LiDAR survey, it is possible to find ecosystems at multiple evolution stages to observe LiDAR patterns variations and eventually link them to structural and functional dynamics. Our results show that species feature distinctive vertical distributions of LiDAR returns that concentrate with crown closure and rise with age. Balsam fir and paper birch had a similar vertical distribution of LiDAR returns, like white spruce and black spruce. Aspen was the most different species with a more uniform distribution of LiDAR returns and a peak in the superior part of the stand. Balsam fir–paper birch displayed a peak centered around 50% of stand height, while the white–black spruces had their distributions skewed below 30% of stand height. Increase in crown closure concentrated the distributions around 50% by deflating the distribution below 33%, while age affected was more diffuse across the whole stand height. These results could improve our understanding of the evolution of the forest structure over changing conditions and could be used for stand-level species classification with LiDAR.

Acknowledgments

We thank Benoît St-Onge, Nicole K. S. Barker, Sébastien Renard, Christian Roy and Josh Nowak for comments on early versions of this manuscript; Tomáš Mrkvička for helpful discussions on the transformations of heteroscedastic data; Anick Patry, Antoine Leboeuf, Marc-Olivier Lemonde, and Jean-François Bourdon from Ministère des Forêts, de la Faune et des Parcs for providing data and support.

Declarations

Funding

This work was supported by the Ministère des Forêts de la Faune et des Parcs du Québec through the Fonds de Recherche Québécois sur la Nature et les Technologies and the Academy of Finland (project numbers 295100 and 327211).

Conflicts of interest/Competing interests

We declare no conflict of interest.

Availability of data and material

The original data was shared and is available upon request to the Gouvernement du Québec. The processed data is available in our repository https://github.com/etiennebr/vertical-lidar-paper

Code availability

The code to perform the analysis is available in a git repository at https://github.com/etiennebr/vertical-lidar-paper

Author contribution statement

ER is the primary author of the manuscript. ER, NCC and JB contributed to the design of the study; the analysis was conducted by ER and MM, the redaction was conducted by ER and revised by other authors; all authors read and approved this version to be published.

References

Aber JD (1979) Foliage-Height Profiles and Succession in Northern Hardwood Forests. Ecology 60:18–23. https://doi.org/10.2307/1936462

Anderson MJ, Robinson J (2001) Permutation Tests for Linear Models. Australian & New Zealand Journal of Statistics 43:75–88. https://doi.org/10.1111/1467-842X.00156

Axelsson A, Lindberg E, Olsson H (2018) Exploring Multispectral ALS Data for Tree Species Classification. Remote Sensing 10:183. https://doi.org/10.3390/rs10020183

Bassow SL, Bazzaz FA (1997) Intra- and inter-specific variation in canopy photosynthesis in a mixed deciduous forest. Oecologia 109:507–515. https://doi.org/10.1007/s004420050111

Beland M, Parker G, Sparrow B et al (2019) On promoting the use of lidar systems in forest ecosystem research. Forest Ecology and Management 450:117484. https://doi.org/10.1016/j.foreco.2019.117484

Breusch TS, Pagan AR (1979) A Simple Test for Heteroscedasticity and Random Coefficient Variation. Econometrica 47:1287–1294. https://doi.org/10.2307/1911963

Budei BC, St-Onge B (2018) Variability of Multispectral Lidar 3D and Intensity Features with Individual Tree Height and Its Influence on Needleleaf Tree Species Identification. Canadian Journal of Remote Sensing 44:263–286. https://doi.org/10.1080/07038992.2018.1478724

Budei BC, St-Onge B, Hopkinson C, Audet F-A (2018) Identifying the genus or species of individual trees using a three-wavelength airborne lidar system. Remote Sensing of Environment 204:632–647. https://doi.org/10.1016/j.rse.2017.09.037

Cao L, Coops NC, Hermosilla T et al (2014) Using Small-Footprint Discrete and Full-Waveform Airborne LiDAR Metrics to Estimate Total Biomass and Biomass Components in Subtropical Forests. Remote Sensing 6:7110–7135. https://doi.org/10.3390/rs6087110

Coops NC, Varhola A, Bater CW et al (2009) Assessing differences in tree and stand structure following beetle infestation using lidar data. Canadian Journal of Remote Sensing 35:497–508. https://doi.org/10.5589/m10-005

Coops N, Hilker T, Wulder M et al (2007) Estimating canopy structure of Douglas-fir forest stands from discrete-return LiDAR. Trees - Structure and Function 21:295–310. https://doi.org/10.1007/s00468-006-0119-6

Crespo-Peremarch P, Fournier RA, Nguyen V-T et al (2020) A comparative assessment of the vertical distribution of forest components using full-waveform airborne, discrete airborne and discrete terrestrial laser scanning data. Forest Ecology and Management 473:118268. https://doi.org/10.1016/j.foreco.2020.118268

De Pury DGG, Farquhar GD (1997) Simple scaling of photosynthesis from leaves to canopies without the errors of big-leaf models. Plant, Cell & Environment 20:537–557. https://doi.org/10.1111/j.1365-3040.1997.00094.x

Ellsworth DS, Reich PB (1993) Canopy structure and vertical patterns of photosynthesis and related leaf traits in a deciduous forest. Oecologia 96:169–178. https://doi.org/10.1007/BF00317729

Falkowski MJ, Evans JS, Martinuzzi S et al (2009) Characterizing forest succession with lidar data: An evaluation for the Inland Northwest, USA. Remote Sensing of Environment 113:946–956. https://doi.org/10.1016/j.rse.2009.01.003

Fassnacht FE, Latifi H, Stereńczak K et al (2016) Review of studies on tree species classification from remotely sensed data. Remote Sensing of Environment 186:64–87. https://doi.org/10.1016/j.rse.2016.08.013

Fedrigo M, Newnham GJ, Coops NC et al (2018) Predicting temperate forest stand types using only structural profiles from discrete return airborne lidar. ISPRS Journal of Photogrammetry and Remote Sensing 136:106–119. https://doi.org/10.1016/j.isprsjprs.2017.11.018

Freedman D, Lane D (1983) A Nonstochastic Interpretation of Reported Significance Levels. Journal of Business & Economic Statistics 1:292–298. https://doi.org/10.1080/07350015.1983.10509354

Harding DJ, Lefsky MA, Parker GG, Blair JB (2001) Laser altimeter canopy height profiles: methods and validation for closed-canopy, broadleaf forests. Remote Sensing of Environment 76:283–297. https://doi.org/10.1016/S0034-4257(00)00210-8

Heinzel J, Koch B (2011) Exploring full-waveform LiDAR parameters for tree species classification. International Journal of Applied Earth Observation and Geoinformation 13:152–160. https://doi.org/10.1016/j.jag.2010.09.010

Heinzel J, Koch B (2012) Investigating multiple data sources for tree species classification in temperate forest and use for single tree delineation. International Journal of Applied Earth Observation and Geoinformation 18:101–110. https://doi.org/10.1016/j.jag.2012.01.025

Hilker T, Leeuwen M van, Coops NC et al (2010) Comparing canopy metrics derived from terrestrial and airborne laser scanning in a Douglas-fir dominated forest stand. Trees 24:819–832. https://doi.org/10.1007/s00468-010-0452-7

Holmgren J, Persson Å (2004) Identifying species of individual trees using airborne laser scanner. Remote Sensing of Environment 90:415–423. https://doi.org/10.1016/S0034-4257(03)00140-8

Hovi A, Korhonen L, Vauhkonen J, Korpela I (2016) LiDAR waveform features for tree species classification and their sensitivity to tree- and acquisition related parameters. Remote Sensing of Environment 173:224–237. https://doi.org/10.1016/j.rse.2015.08.019

Isenburg M (2012) LAStools - efficient tools for LiDAR processing. Version 120301URL http://lastools.org

Kim S, Hinckley T, Briggs D (2011) Classifying individual tree genera using stepwise cluster analysis based on height and intensity metrics derived from airborne laser scanner data. Remote Sensing of Environment 115:3329–3342. https://doi.org/10.1016/j.rse.2011.07.016

Koenig K, Höfle B (2016) Full-Waveform Airborne Laser Scanning in Vegetation Studies—A Review of Point Cloud and Waveform Features for Tree Species Classification. Forests 7:198. https://doi.org/10.3390/f7090198

Korhonen L, Korpela I, Heiskanen J, Maltamo M (2011) Airborne discrete-return LIDAR data in the estimation of vertical canopy cover, angular canopy closure and leaf area index. Remote Sensing of Environment 115:1065–1080. https://doi.org/10.1016/j.rse.2010.12.011

Lacointe A (2000) Carbon allocation among tree organs: a review of basic processes and representation in functional-structural tree models. Annals of Forest Science 57:521–533. https://doi.org/10.1051/forest:2000139

Lefsky MA, Cohen WB, Harding DJ et al (2002) Lidar remote sensing of above-ground biomass in three biomes. Global Ecology and Biogeography 11:393–399. https://doi.org/10.1046/j.1466-822x.2002.00303.x

MacArthur RH, Horn HS (1969) Foliage Profile by Vertical Measurements. Ecology 50:802–804

Magnussen S, Eggermont P, LaRiccia VN (1999) Recovering Tree Heights from Airborne Laser Scanner Data. Forest Science 45:407–422

Maltamo M, Packalén P, Yu X et al (2005) Identifying and quantifying structural characteristics of heterogeneous boreal forests using laser scanner data. Forest Ecology and Management 216:41–50. https://doi.org/10.1016/j.foreco.2005.05.034

Martin-Ducup O, Schneider R, Fournier RA (2016) Response of sugar maple (Acer saccharum, Marsh.) tree crown structure to competition in pure versus mixed stands. Forest Ecology and Management 374:20–32. https://doi.org/10.1016/j.foreco.2016.04.047

Mehtätalo L (2006) Eliminating the effect of overlapping crowns from aerial inventory estimates. Can J For Res/Rev can rech for 36:1649–1660

Mrkvička T, Myllymäki M, Jílek M, Hahn U (2020) A one-way ANOVA test for functional data with graphical interpretation. Kybernetika 432–458. https://doi.org/10.14736/kyb-2020-3-0432

Mrkvička T, Roskovec T, Rost M (2019) A Nonparametric Graphical Tests of Significance in Functional GLM. Methodol Comput Appl Probab. https://doi.org/10.1007/s11009-019-09756-y

MRNQ (2007) Norme de photo-interprétation (version provisoire). Direction des inventaires forestiers, Gouvernement du Québec

Muss JD, Mladenoff DJ, Townsend PA (2011) A pseudo-waveform technique to assess forest structure using discrete lidar data. Remote Sensing of Environment 115:824–835. https://doi.org/10.1016/j.rse.2010.11.008

Myllymäki M, Mrkvička T (2019) GET: Global envelopes in R. arXiv:191106583 [stat]

Myllymäki M, Mrkvička T, Grabarnik P et al (2017) Global envelope tests for spatial processes. Journal of the Royal Statistical Society B 79:381–404. https://doi.org/10.1111/rssb.12172

Palace MW, Sullivan FB, Ducey MJ et al (2015) Estimating forest structure in a tropical forest using field measurements, a synthetic model and discrete return lidar data. Remote Sensing of Environment 161:1–11. https://doi.org/10.1016/j.rse.2015.01.020

Papa D de A, Almeida DRA de, Silva CA et al (2020) Evaluating tropical forest classification and field sampling stratification from lidar to reduce effort and enable landscape monitoring. Forest Ecology and Management 457:117634. https://doi.org/10.1016/j.foreco.2019.117634

Parker GG, Harmon ME, Lefsky MA et al (2004) Three-dimensional structure of an old-growth Pseudotsuga-Tsuga canopy and its implications for radiation balance, microclimate, and gas exchange. Ecosystems 7:440–453

Pretzsch H, Dieler J (2012) Evidence of variant intra- and interspecific scaling of tree crown structure and relevance for allometric theory. Oecologia 169:637–649. https://doi.org/10.1007/s00442-011-2240-5

Purves DW, Lichstein JW, Pacala SW (2007) Crown Plasticity and Competition for Canopy Space: A New Spatially Implicit Model Parameterized for 250 North American Tree Species. PLoS ONE 2:e870. https://doi.org/10.1371/journal.pone.0000870

Racine EB, Coops NC, St-Onge B, Bégin J (2014) Estimating Forest Stand Age from LiDAR-Derived Predictors and Nearest Neighbor Imputation. Forest Science 60:128–136. https://doi.org/http://dx.doi.org/10.5849/forsci.12-088

Ramsay J, Silverman BW (2005) Functional data analysis, 2nd edn. Springer, New York

Räty J, Vauhkonen J, Maltamo M, Tokola T (2016) On the potential to predetermine dominant tree species based on sparse-density airborne laser scanning data for improving subsequent predictions of species-specific timber volumes. For Ecosyst 3:1. https://doi.org/10.1186/s40663-016-0060-0

R Core Team (2020) R: A Language and Environment for Statistical Computing version 3.6.3. R Foundation for Statistical Computing, Vienna, Austria

Riggins JJ, Tullis JA, Stephen FM (2009) Per-segment Aboveground Forest Biomass Estimation Using LIDAR-Derived Height Percentile Statistics. GIScience & Remote Sensing 46:232–248. https://doi.org/10.2747/1548-1603.46.2.232

Roussel J-R, Béland M, Caspersen J, Achim A (2018) A mathematical framework to describe the effect of beam incidence angle on metrics derived from airborne LiDAR: The case of forest canopies approaching turbid medium behaviour. Remote Sensing of Environment 209:824–834. https://doi.org/10.1016/j.rse.2017.12.006

Roussel J-R, Caspersen J, Béland M et al (2017) Removing bias from LiDAR-based estimates of canopy height: Accounting for the effects of pulse density and footprint size. Remote Sensing of Environment 198:1–16. https://doi.org/10.1016/j.rse.2017.05.032

Seavy NE, Viers JH, Wood JK (2009) Riparian bird response to vegetation structure: a multiscale analysis using LiDAR measurements of canopy height. Ecological Applications 19:1848–1857. https://doi.org/10.1890/08-1124.1

Stark SC, Leitold V, Wu JL et al (2012) Amazon forest carbon dynamics predicted by profiles of canopy leaf area and light environment. Ecology Letters 15:1406–1414. https://doi.org/10.1111/j.1461-0248.2012.01864.x

Tackenberg O (2007) A New Method for Non-destructive Measurement of Biomass, Growth Rates, Vertical Biomass Distribution and Dry Matter Content Based on Digital Image Analysis. Ann Bot 99:777–783. https://doi.org/10.1093/aob/mcm009

Thorpe HC, Astrup R, Trowbridge A, Coates KD (2010) Competition and tree crowns: A neighborhood analysis of three boreal tree species. Forest Ecology and Management 259:1586–1596. https://doi.org/10.1016/j.foreco.2010.01.035

Vaughn NR, Moskal LM, Turnblom EC (2012) Tree Species Detection Accuracies Using Discrete Point Lidar and Airborne Waveform Lidar. Remote Sensing 4:377–403. https://doi.org/10.3390/rs4020377

Vierling KT, Bässler C, Brandl R et al (2010) Spinning a laser web: predicting spider distributions using LiDAR. Ecological Applications 21:577–588. https://doi.org/10.1890/09-2155.1

Vierling KT, Vierling LA, Gould WA et al (2008) Lidar: shedding new light on habitat characterization and modeling. Frontiers in Ecology and the Environment 6:90–98. https://doi.org/10.1890/070001

White JC, Wulder MA, Varhola A et al (2013) A best practices guide for generating forest inventory attributes from airborne laser scanning data using an area-based approach. The Forestry Chronicle 89:722–723. https://doi.org/10.5558/tfc2013-132

Winkler AM, Ridgway GR, Webster MA et al (2014) Permutation inference for the general linear model. NeuroImage 92:381–397. https://doi.org/10.1016/j.neuroimage.2014.01.060

Wulder MA, White JC, Nelson RF et al (2012) Lidar sampling for large-area forest characterization: A review. Remote Sensing of Environment 121:196–209. https://doi.org/10.1016/j.rse.2012.02.001

Ørka HO, Næsset E, Bollandsås OM (2009) Classifying species of individual trees by intensity and structure features derived from airborne laser scanner data. Remote Sensing of Environment 113:1163–1174. https://doi.org/10.1016/j.rse.2009.02.002